Spectral Color Correction based on Linear Estimation

Christian Münzenmayer[1], Thomas Wittenberg[1], and Dietrich Paulus[2]

[1] Fraunhofer Institut für Integrierte Schaltungen,
Am Wolfsmantel 33, D-91058 Erlangen
{mzn,wbg}@iis.fraunhofer.de
[2] Universität Koblenz-Landau, Institut für Computervisualistik,
Universitätsstraße 1, D-56070 Koblenz
paulus@uni-koblenz.de

Abstract

This paper reviews a new spectral approach to color correction which can be used e.g. in medical image analysis applications. The proposed method is based on linear estimation of all spectral components of a color imaging system, consisting of the spectral sensitivity of the sensor, the spectral radiance of the illuminant and the spectral reflectances of the surfaces within the scene. In particular, constrained principal eigenvector and Wiener inverse estimation are used for this estimation A piecewise linear interpolation step is used to handle non-linearities of the imaging device.

The novelty of the approach lies in the generalization of the image formation model by dropping the positivity constraint usually imposed by other calibration methods. Thus, this method can be applied to camera systems with internal color value matrixing. Experimental results are presented from a data set acquired by a commercial video endoscopy system for medical imaging.

1 Introduction

Human observers of color images are well trained to implicitly correct various and varying color phenomena. Some examples of such phenomena are non-uniform illumination, changing surface characteristics or changing color temperature, e.g. by aging light sources. For automated image analysis systems to work properly, these adaption capabilities have to be emulated by suitable algorithms. In this contribution a solution to the problem of global color temperature changes is presented. We determine the illumination spectrum of a scene by measuring the color sensor's response to a standard color target (e.g. IT8.7) combined with a linear estimation of the spectrum. Calibration of the camera and illumination spectrum estimation is based on a constrained principal eigenvector approximation, while spectral surface reflectivities are determined by Wiener inverse estimation.

The novelty of our approach lies in the generalization of the image formation model allowing for linear pre-processing inside the camera system. Such transforms would usually lead to erroneous results with positivity constraint based algorithms such as [12, 2, 1] or a monochromator based measurement as pointed in [6]. This effect is also confirmed by our experimental results. In contrast to other authors we explicitly model the so-called *matrixing* of the raw sensor's response inside the camera. Furthermore, most cameras have a non-linear response which can also be corrected in our framework by piecewise linear interpolation. A more detailed account of our method can be found in [8].

This paper is organized as follows. First, in Section 2 the linear image formation model will be introduced. In Section 3, the color correction framework will be described in a top-down approach starting with an overview of the algorithm supplemented by some details about the

linear estimation methods. The experimental part in Section 4 describes the data acquisition, camera calibration and spectral estimation procedure. Final results in comparison with other algorithms are presented and discussed in Section 5. We summarize with a short discussion in Section 6.

2 Image Formation Model

Image formation is usually modeled as a linear process where the sensor response $\rho^{(k)} \in \mathbb{R}$ for the k'th spectral band is the result of the integration of spectral radiance of a light source $E(\lambda)$ with wavelength λ, the spectral reflectivity of the surface $s_{\boldsymbol{w}}(\lambda)$ at some scene point $\boldsymbol{w} \in \mathbb{R}^3$ and the sensor's sensitivities $R^{(k)}(\lambda)$. The absolute magnitude of the linear sensor response for a pixel $\boldsymbol{x} \in \mathbb{R}^2$ for matte Lambertian surfaces is determined by the scalar product between the emitting light source vector $\boldsymbol{e}(\boldsymbol{w})$ and the surface normal vector $\boldsymbol{n}(\boldsymbol{w})$ together with the integration time t_{I}:

$$\rho^{(k)}(\boldsymbol{x}) = t_{\mathrm{I}} \boldsymbol{e}(\boldsymbol{w}) \boldsymbol{n}(\boldsymbol{w}) \int_{\lambda} R^{(k)}(\lambda) E(\lambda) s(\boldsymbol{w}, \lambda) d\lambda + \eta(\boldsymbol{x}) \quad . \tag{1}$$

Most often the dark current $\eta(\boldsymbol{x})$ is already corrected for in modern camera systems. Assuming controlled illumination conditions, camera integration time and geometry-dependent terms will be dropped for the further analysis. Formulated in matrix notation (with matrix sizes in subscript $M \times N$ format, i.e. M rows and N columns), the discretized version of this model can be written as

$$\boldsymbol{\rho}_{K\times 1} = (\boldsymbol{R}_{L\times K})^{\mathrm{T}} \boldsymbol{E}_{L\times L} \boldsymbol{s}_{L\times 1} \tag{2}$$

for K spectral bands and L discrete samples with the sensor sensitivity matrix $\boldsymbol{R}$, the diagonal illumination matrix $\boldsymbol{E}$ and the surface reflectivity vector $\boldsymbol{s}$. To account for the internal processing common to modern digital cameras, a $K \times K$ camera matrix $\boldsymbol{M}_{\mathrm{C}}$ will be introduced into the modified image formation model, formulated in vector form as

$$\boldsymbol{\rho}(\boldsymbol{x}) = \boldsymbol{M}_{\mathrm{C}} t_{\mathrm{I}} \boldsymbol{e}(\boldsymbol{w}) \boldsymbol{n}(\boldsymbol{w}) \int_{\lambda} \boldsymbol{R}_{\circ}(\lambda) E(\lambda) s(\boldsymbol{w}, \lambda) d\lambda \tag{3}$$

with the K-vector of sensor responses $\boldsymbol{\rho}$ and the raw sensor sensitivity as K-vector $\boldsymbol{R}_{\circ}(\lambda)$. For numerical solution the *discrete image formation model* (2) will be used, with the effective sensor sensitivity matrix $\boldsymbol{R} = \boldsymbol{R}_{\circ} \boldsymbol{M}_{\mathrm{C}}$, the diagonal illumination matrix $\boldsymbol{E}$ and the L-element surface reflectance vector $\boldsymbol{s}$.

3 Spectral Color Correction

Spectral color correction (SPC) is a color constancy mapping which makes use of a fully calibrated sensor as well as estimates of illuminant and surface reflectance spectra. Sensor responses are related by (2) assuming that the surface reflectance L-vector $\boldsymbol{s}$ is unchanging in

$$\boldsymbol{\rho}^{\mathrm{U}} = (\boldsymbol{R}^{\mathrm{U}})^T \boldsymbol{E}^{\mathrm{U}} \boldsymbol{s} \rightarrow \boldsymbol{\rho}^{\mathrm{C}} = (\boldsymbol{R}^{\mathrm{C}})^T \boldsymbol{E}^{\mathrm{C}} \boldsymbol{s} \quad . \tag{4}$$

Superscripts U denote uncalibrated factors, while the superscripts C describe canonical factors. Based on these relationships the surface reflectance $\boldsymbol{s}$ has to be recovered from the sensor response $\boldsymbol{\rho}^{\mathrm{U}}$, the sensor characteristic $\boldsymbol{R}^{\mathrm{U}}$, and the illumination spectrum $\boldsymbol{E}^{\mathrm{U}}$. In many practical applications only the illuminant spectra $\boldsymbol{E}^{\mathrm{U}}$ differ, while the camera response remains unchanged, i.e. $\boldsymbol{R}^{\mathrm{U}} = \boldsymbol{R}^{\mathrm{C}}$.

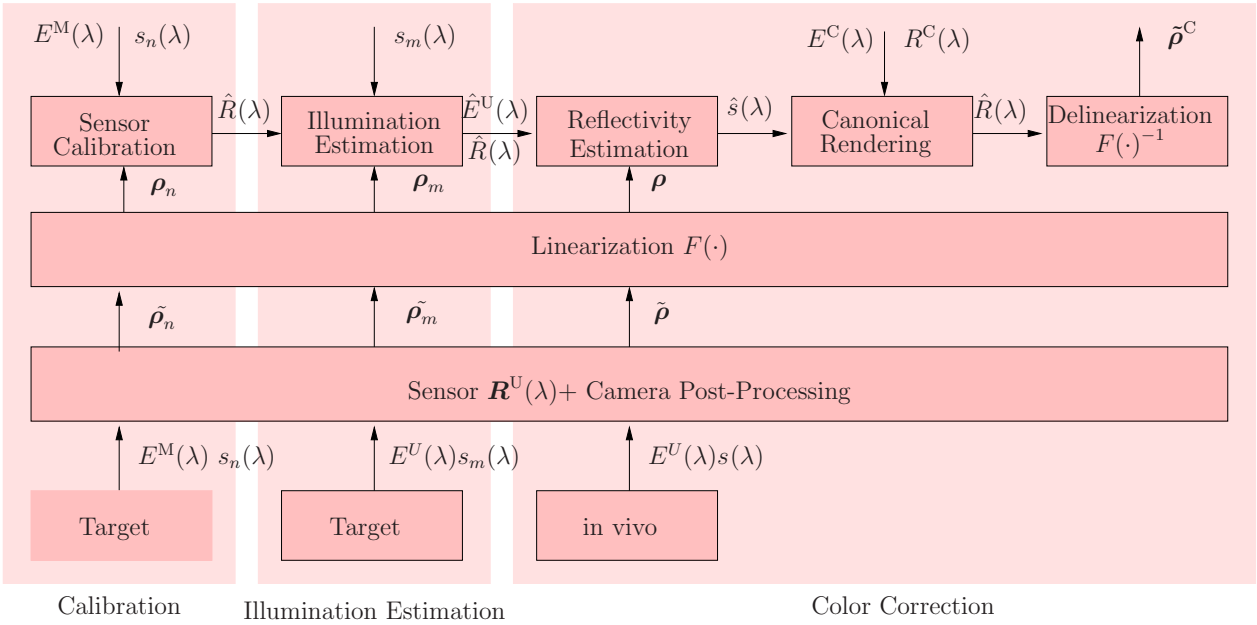

Figure 1: Spectral color correction scheme providing color constancy for medical applications based on a linear image formation model and linear estimators. The model explicitly assumes cameras with non-linear post-processing and linear color correction matrix. Scenes can be rendered with arbitrary sensor characteristics and any assumed illumination. Sensor calibration and computation of the linearization function has to be done once for each camera device.

First, an overview of the *SPC* algorithm is depicted in Figure 1 which will be further explained in the following sections of this text. The image formation process starts in the bottom section of the sketch where the color signals $E(\lambda)s(\lambda)$, consisting of the reflected incident illumination $E(\lambda)$ by the surface with reflectivity $s(\lambda)$, are captured by the camera. The non-linear response $\tilde{\rho}$ results from the linear raw sensor sensitivity $R_\circ(\lambda)$ and some generally unknown camera post-processing which is often a color correction matrix $\boldsymbol{M}_{\mathrm{C}}$ correcting for filter insufficiencies and a non-linear gamma correction. Non-linearities of the camera system are captured by a linearization function $F(\cdot)$ converting the non-linear response $\tilde{\rho}$ to an ideal linear response

$$\rho^{(k)} = F(\tilde{\rho}^{(k)}) \tag{5}$$

by radiometric calibration [3].

The sensor calibration delivers an estimate $\hat{R}(\lambda)$ of the effective sensor sensitivity curves of the camera including any color correction matrix $\boldsymbol{M}_{\mathrm{C}}$ which might be present in the camera hardware. This estimation requires the acquisition of a color reference target with known reflectivities $s_n(\lambda)$ for $n = [0; N-1]$ color patches under known measurement illumination conditions denoted by $E^{\mathrm{M}}(\lambda)$ (Section 3.1). To correct a series of images, an estimate of the unknown illumination $\hat{E}^{\mathrm{U}}(\lambda)$ can be derived from the sensor estimate $\hat{R}(\lambda)$ and color references $\boldsymbol{\rho}_m$ with corresponding measured surface reflectivities $s_m(\lambda)$ (Section 3.2). Note that these $m = [0; M-1]$ color patches can be totally different from the ones used for the sensor calibration. With estimates available for the sensor $\hat{R}(\lambda)$ and for the unknown illumination $\hat{E}^{\mathrm{U}}(\lambda)$, the actual surface spectrum $\hat{s}(\lambda)$ for each color pixel $\boldsymbol{\rho}$ of the in vivo images can be derived (Section 3.3). The canonical rendering is the straight-forward application of the discrete image formation model (2) with a canonical sensor model $R^{\mathrm{C}}(\lambda)$ and illumination $E^{\mathrm{C}}(\lambda)$ which could be one of the CIE standard daylight illuminations, e.g. D65. If the original imaging device characteristic is required, the inverse linearization function $F^{-1}(\cdot)$ can be applied leading to the illumination and gamma corrected $\tilde{\boldsymbol{\rho}}^{\mathrm{C}}$.

3.1 Color Calibration of the Camera System

Color calibration of a camera system will be understood as the estimation of the *effective spectral sensitivity* of the complete system including lenses, color filters and the CCD sensor. All these are part of an internal processing chain within the camera, yielding the acquired digital image. Therefore, calibration results may certainly differ from the results of a mere color filter measurement which does not include any possible color processing in the camera system. To estimate the discrete sensor characteristic $\boldsymbol{R}$, N reference sensor responses $\boldsymbol{\rho}_n$ are acquired from a color calibration target (e.g. IT8.7). The corresponding spectral reflectances $\boldsymbol{s}_n$ with L discrete samples will be arranged into a $L \times N$ matrix $\boldsymbol{S}$. The illumination charateristics $\boldsymbol{E}$ have to be measured with a spectro-radiometer. With modifications, the constrained principal eigenvector approach can be applied to solve the inverse problem as derived in [9]. Without loss of generality the sensor responses $\boldsymbol{\rho}_n$ for $K = 3$ filters will be arranged into a column vector of NK elements

$$\boldsymbol{v} = \begin{pmatrix} \rho_{\mathrm{R},1} & \rho_{\mathrm{G},1} & \rho_{\mathrm{B},1} & \cdots & \rho_{\mathrm{R,N}} & \rho_{\mathrm{G,N}} & \rho_{\mathrm{B,N}} \end{pmatrix}^T \tag{6}$$

and the products of the corresponding surface reflectances in matrix $\boldsymbol{S}$ with the measurement illumination spectrum $\boldsymbol{E}$ into a matrix

$$\boldsymbol{C}_{NK\times KL} = \begin{pmatrix} E_1S_{1,1} & \cdots & E_LS_{L,1} & 0 & \cdots & 0 & 0 & \cdots & 0 \\ 0 & \cdots & 0 & E_1S_{1,1} & \cdots & E_LS_{L,1} & 0 & \cdots & 0 \\ 0 & \cdots & 0 & 0 & \cdots & 0 & E_1S_{1,1} & \cdots & E_LS_{L,1} \\ \vdots & \vdots & \vdots & \vdots & \vdots & \vdots & \vdots & \vdots & \vdots \\ E_1S_{1,N} & \cdots & E_LS_{L,N} & 0 & \cdots & 0 & 0 & \cdots & 0 \\ 0 & \cdots & 0 & E_1S_{1,N} & \cdots & E_LS_{L,N} & 0 & \cdots & 0 \\ 0 & \cdots & 0 & 0 & \cdots & 0 & E_1S_{1,N} & \cdots & E_LS_{L,N} \end{pmatrix} . \tag{7}$$

Arranging the sensor sensitivities into a column vector $\boldsymbol{r}$ with KL elements, the image formation expression (2) can be reformulated as

$$\boldsymbol{v} = \boldsymbol{C}\boldsymbol{r} \tag{8}$$

which allows a formulation of the regularized inversion. Regularization is achieved by applying additional constraints to the well-known principal eigenvector approach [3] similar to [9]. First, the illumination and surface matrix $\boldsymbol{C}$ is decomposed by a singular value decomposition $\boldsymbol{C} = \boldsymbol{U}\boldsymbol{\Sigma}\boldsymbol{V}^T$. The principal eigenvector approach is implemented using a diagonal matrix $\boldsymbol{P} = [P_{ij}]_{i,j=1\ldots L}$, where the first r diagonal elements $P_{ij} = 1$ for $i = j$, and the rest of the matrix contains 0 everywhere else. The parameter r will be called the rank parameter. Further regularization of (8) is achieved by defining a $L \times L$ constraint matrix $\tilde{\boldsymbol{D}}$ which is applied to each of the K filters by $\boldsymbol{D}$:

$$\tilde{\boldsymbol{D}} = \begin{pmatrix} 1 & -1 & 0 & 0 & \cdots & \cdots & 0 \\ -1 & 2 & -1 & 0 & \cdots & \cdots & 0 \\ 0 & -1 & 2 & -1 & 0 & \cdots & 0 \\ \vdots & & & & & & \\ 0 & \cdots & 0 & -1 & 2 & -1 & 0 \\ 0 & \cdots & \cdots & 0 & -1 & 2 & -1 \\ 0 & \cdots & \cdots & \cdots & 0 & -1 & 1 \end{pmatrix}, \quad \boldsymbol{D} = \begin{pmatrix} \tilde{\boldsymbol{D}}' & \boldsymbol{0} & \cdots & \boldsymbol{0} \\ \boldsymbol{0} & \tilde{\boldsymbol{D}}' & \cdots & \boldsymbol{0} \\ \vdots & \vdots & \ddots & \vdots \\ \boldsymbol{0} & \boldsymbol{0} & \cdots & \tilde{\boldsymbol{D}}' \end{pmatrix}. \tag{9}$$

As in [9], this matrix needs to be slightly modified to avoid singularity of the solution by defining $d_{1,2} = 0$ and $d_{L,L-1} = 0$, yielding $\tilde{\boldsymbol{D}}'$. With these preparations the sensor response follows from the regularized estimation

$$\hat{\boldsymbol{r}}_{\mathrm{C}} = (\boldsymbol{V}\boldsymbol{P}\boldsymbol{\Sigma}^2\boldsymbol{V}^T + \mu\boldsymbol{D})^{-1}\boldsymbol{V}\boldsymbol{P}\boldsymbol{\Sigma}\boldsymbol{U}^T\boldsymbol{v} \tag{10}$$

with μ controlling the amount of the regularization. The estimated sensor matrix $\hat{\boldsymbol{R}}_{\mathrm{C}}$ is constructed by re-arranging the stacked representation from the column vector $\hat{\boldsymbol{r}}_{\mathrm{C}}$.

3.2 Estimation of Illumination Spectrum

To recover the illumination spectrum, knowledge of the sensor characteristic $\boldsymbol{R}$ and a distinct number of M reference sensor responses $\boldsymbol{\rho}_m$ with their corresponding reflectances $\boldsymbol{s}_m$ arranged into a $L \times M$ matrix $\boldsymbol{S}$ are required. Therefore, an image of a calibration target (e.g. IT8.7) under the same illumination conditions is required to extract reference sensor responses $\boldsymbol{\rho}_m$. To solve this tremendeously ill-conditioned system, an adapted *constrained principal eigenvector* method and a *Wiener inverse* approach is described. The products of the target's surface reflectances $\boldsymbol{S}$ with the device sensitivities $\boldsymbol{R}$ are combined into a matrix $\boldsymbol{A}$

$$\boldsymbol{A}_{NK\times L} = \begin{pmatrix} R_{\mathrm{R},1}S_{1,1} & R_{\mathrm{R},2}S_{2,1} & \cdots & R_{\mathrm{R},L}S_{L,1} \\ R_{\mathrm{G},1}S_{1,1} & R_{\mathrm{G},2}S_{2,1} & \cdots & R_{\mathrm{G},L}S_{L,1} \\ R_{\mathrm{B},1}S_{1,1} & R_{\mathrm{B},2}S_{2,1} & \cdots & R_{\mathrm{B},L}S_{L,1} \\ \vdots & \vdots & & \vdots \\ R_{\mathrm{R},1}S_{1,N} & R_{\mathrm{R},2}S_{2,N} & \cdots & R_{\mathrm{R},L}S_{L,N} \\ R_{\mathrm{G},1}S_{1,N} & R_{\mathrm{G},2}S_{2,N} & \cdots & R_{\mathrm{G},L}S_{L,N} \\ R_{\mathrm{B},1}S_{1,N} & R_{\mathrm{B},2}S_{2,N} & \cdots & R_{\mathrm{B},L}S_{L,N} \end{pmatrix} . \tag{11}$$

Writing the illumination spectrum as a vector $\boldsymbol{e}_{L\times 1}$ the discrete image formation expression (2) can be formulated as $\boldsymbol{v} = \boldsymbol{A}\boldsymbol{e}$. The arrangement of the sensor responses in a column vector is $\boldsymbol{v}$ identical to (6), which allows formulation of the regularized inversion as well.

Regularization is also based on singular value decomposition of the sensor and surface matrix $\boldsymbol{A} = \boldsymbol{U}\boldsymbol{\Sigma}\boldsymbol{V}^T$ and a rank restriction up to r eigenvectors. The condition of the smoothing matrix $\tilde{\boldsymbol{D}}$ will be enhanced as suggested in [4] by adding an identity matrix scaled by a coefficient ν. An estimate for the illumination spectrum can be determined from

$$\hat{\boldsymbol{e}}_{\mathrm{C}} = (\boldsymbol{V}\boldsymbol{P}\boldsymbol{\Sigma}^2\boldsymbol{V}^T + \mu\tilde{\boldsymbol{D}} + \nu\boldsymbol{I})^{-1}\boldsymbol{V}\boldsymbol{P}\boldsymbol{\Sigma}\boldsymbol{U}^T\boldsymbol{v} \tag{12}$$

with μ, ν and r controlling the regularization. Should there be any negative values in the estimate $\hat{\boldsymbol{e}}_{\mathrm{C}}$, clipping can be applied.

3.3 Estimation of Surface Reflectivity Spectrum

Clearly, the estimation of surface reflectivity spectra with e.g. $L = 31$ sample points (representing the visible wavelength domain from 400 to 700 nm with intervals of $\Delta\lambda = 10$ nm) from the image acquisition parameters $\boldsymbol{R}$, $\boldsymbol{E}$ and the sensor responses $\boldsymbol{\rho}$ from only $K = 3$ channels is underdetermined. From the image formation model (2) we derive the simplified notation $\boldsymbol{\rho}_{K\times 1} = \boldsymbol{B}_{K\times L}\boldsymbol{s}_{L\times 1}$ with an illumination and sensor matrix $\boldsymbol{B}_{K\times L} = (\boldsymbol{R}_{L\times K})^T\boldsymbol{E}_{L\times L}$. This matrix has maximal rank $K = 3$ for standard video cameras with RGB filters. Therefore, the rank limitation used in the constrained principal eigenvector approach is not helpful here. This leaves the option of using the Wiener inverse estimate suggested by Pratt et al. [10].

The Wiener inverse method requires an estimate of the correlation matrix $\boldsymbol{R}_{ss}$. If a representative set of N surface spectra is available, it can be used to build the correlation matrix by $\boldsymbol{R}_{ss} = \boldsymbol{S}\boldsymbol{S}^T$ with $\boldsymbol{S}$ being a $L \times N$ matrix holding N column vectors of surface spectra. The first-order *Markov covariance matrix* $\hat{\boldsymbol{R}}_{ss} = [\rho^{|i-j|}]_{i,j=1\ldots L}$ can be a useful replacement, if no such references are available [10]. Finally, the Wiener estimate of the surface spectrum is defined as

$$\tilde{\boldsymbol{s}}_{\mathrm{W}} = \boldsymbol{R}_{ss}\boldsymbol{B}^T(\boldsymbol{B}\boldsymbol{R}_{ss}\boldsymbol{B}^T)^{-1}\boldsymbol{\rho} \quad . \tag{13}$$

Negative values in the resulting reflectivety $\tilde{\boldsymbol{s}}_{\mathrm{W}}$ which are due to minor numerical instabilities will be clipped.

4 Experimental Evaluation

In this section we will present an experimental evaluation of our approach using a data set of medical endoscopic images.

4.1 Data Acquisition

Before any measurements were taken, the *automatic gain control (*AGC*)* of the endoscopy system was deactivated and a manual *white-balance* was conducted on the video processor. Measurements of the light source characteristics were performed using a spectroradiometer (Jeti specbos 1100[3]). Correction of the sensor's non-linearity was conducted with the gray-level patches at the bottom of an IT8.7 color reference target by piecewise logarithmic regression as described in [3, 8].

From the 288 color patches on the IT8.7 target the 40 most significant ones were chosen by iteratively adding those spectra with maximal linear independency [3]. The number 40 was chosen as a compromise between accuracy and economy in experimental effort because each patch had to be recorded separately for maximally uniform illumination and to provide enough pixels for averaging the measured sensor response. The first 20 patches are denoted as the *reconstruction set* $\mathfrak{P}_{\mathrm{R}}$ while the following 20 patches represent the *verification set* $\mathfrak{P}_{\mathrm{V}}$. The reconstruction set $\mathfrak{P}_{\mathrm{R}}$ was used to estimate the sensor model and calculate un-biased quality measures with the verification set $\mathfrak{P}_{\mathrm{V}}$ to verify the generalization capabilities of the sensor model.

The reference image with the Olympus GIF-Q160Z gastroscope was acquired in a dark room. With the two light fiber bundles on both sides of the optical channel at the tip of the endoscope an approximate 45/0 geometry was obtained as proposed by the CIE. From the center of the acquired images with the gastroscope in full zoom mode, a 256×256 pixel region of interest was selected, excluding the specular highlights caused by the light fibers. To ensure the validity of the linear image formation model care was taken to avoid clipping of sensor values.

4.2 Sensor Sensitivity Calibration

To find applicable parameters for the estimation methods, three quality measures were used. These are the *root mean square error (RMSE)* ε_ρ, the L2 error measure in the normalized chromaticity space $\varepsilon_{\bar{\rho}}$, and the *normalized cross-correlation (NCC)* c_ρ between ideal and

[3]JETI Technische Instrumente GmbH, D-07745 Jena, http://www.jeti.com

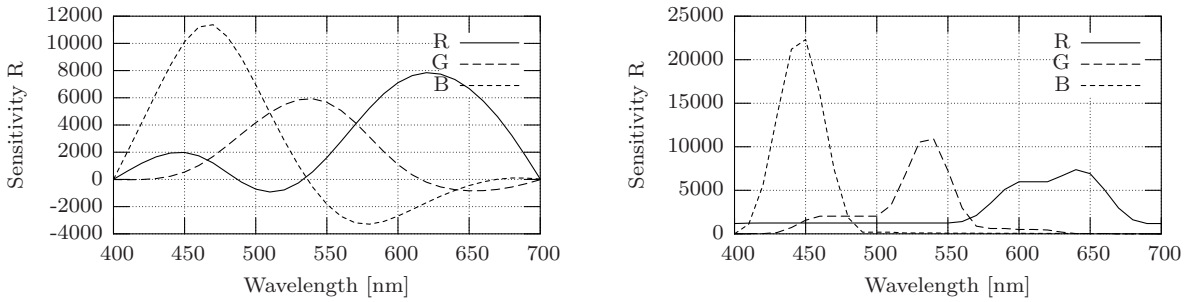

(a) Linear estimate (b) Quadratic programming

Figure 2: (a) Linear estimate of sensor sensitivities $\hat{\boldsymbol{R}}$ of Olympus Evis Exera system obtained by a reference image of an IT8.7 color target and a measurement of the illumination spectrum with $\mu_* = 0.00001$ and $r_* = 20$. (b) shows the estimate of the quadratic programming approach [2].

measured response $\boldsymbol{\rho}^{\mathrm{I}}$ and $\boldsymbol{\rho}^{\mathrm{M}}$. Averaged results of reconstruction and verification data set are denoted by $\overline{\varepsilon_\rho}$, $\overline{\varepsilon_{\bar{\rho}}}$, and $\overline{c_\rho}$, respectively.

The estimation of the sensor sensitivities $R^{(k)}(\lambda)$ is based on the linearized sensor responses of the reconstruction set $\mathfrak{P}_{\mathrm{R}}$, the known reflectance data of the color reference target and the measured spectrum of the light source. For these measurements the estimation parameters have been optimized with respect to the error measures mentioned above. It should be noted that an estimation based on the back-projection error is biased because it has a strong tendency to optimize for the measurement data but not for the real sensor sensitivities. Therefore, the distinct verification set $\mathfrak{P}_{\mathrm{V}}$ was evaluated as an ojective control. Best results in terms of normalized error with $\overline{\varepsilon_{\bar{\rho}}} = 0.061$ were achieved with a regularization of $\mu_* = 0.00001$ (see Figure 2(a)).

These results were also compared with the *quadratic programming* approach by Finlayson et al. [2] which enforces positivity and needs to be parameterized by the number of modes, a weaker form of the so-called *uni-modality* constraint. For the present data set this resulted in high absolute and chromaticity errors ($\overline{\varepsilon_\rho} = 10.37$, $\overline{\varepsilon_{\bar{\rho}}} = 0.086$), see Figure 2(b). However, as already mentioned these constraints cannot be applied when a color correction matrix is built into the camera system which explains the unsatisfactory results. As mentioned in Section 2, the negative sensitivities displayed in Figure 2(a) can be explained by a matrix $\boldsymbol{M}_{\mathrm{C}}$ within the camera system.

4.3 Illumination and Surface Reflectivity Estimation

The presented approach to color correction is based on measurements of the sensor's responses to multiple color patches on a color reference target. With measured spectral reflectivities of these patches and the known sensor model $\boldsymbol{R}$, an estimate of the spectral distribution of the illumination can be obtained. Results will be presented for the constrained principal eigenvector method, which will be compared with the spectroradiometer measurement and evaluated with the back-projection error in device RGB space.

With not much variation in the results when varying the parameters, a correlation to the illumination measurement of $c_{\mathrm{E}} = 0.99$ could be obtained (Figure 3(a)).

Estimating a surface spectrum from the sensor's tristimulus values is a difficult problem to solve, as can be seen from Sect. 3.2. There exist a lot of different results and opinions in literature on how many color filters are needed for an optimal multispectral image acquisition. These values range between $K = \{3, 5, 7\}$ and up to $K = 16$, depending on the applications

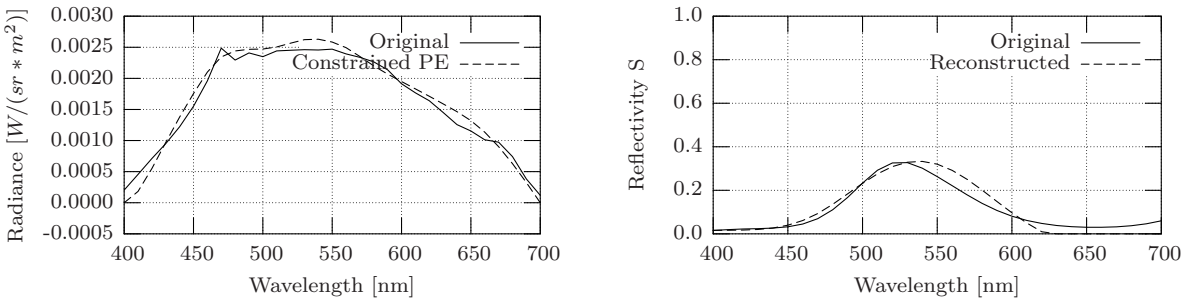

(a) Illumination Spectrum Estimation (b) $P_5 = J18$ ($\Delta E^*_{ab} = 3.31$, $\varepsilon_\rho = 2.25$)

Figure 3: (a) Estimate of illumination spectrum from reconstruction set with $\mu_* = 0.00001$, $r_* = 3$, $\nu_* = 0.1$ compared with reference measurement. (b) Estimate of surface spectrum of a green color patch (J18) from the reconstruction set with Wiener inverse method ($\rho = 0.99$).

and environments at hand [3]. In the present experiments, the image acquisition devices were standard digital video endoscopy systems with $K = 3$ color filters as a fixed limitation of the system. However, for the correction of endoscopic or dermatoscopic imagery, it was shown by principal component analysis, that three principal components are enough to represent 99% of the examined mucousal and skin spectra [7]. Therefore, one can conclude that it should be possible to approximate the surface spectrum well enough for color correction in the device RGB space. The Wiener inverse method was evaluated with a trained correlation matrix $\boldsymbol{R}_{ss} = \boldsymbol{S}\boldsymbol{S}^T$ and the first-order Markov covariance matrix $\hat{\boldsymbol{R}}_{ss}$ with different settings for the correlation parameter ρ. Figure 3(b) shows the estimated surface spectrum compared with the reference measurement for a green color patch (J18) from the reconstruction set.

5 Results

To validate the *SPC* approach in comparison with other methods, color correction was performed on the verification data set $\mathfrak{P}_\mathrm{V}$. Furthermore, the absolute root mean square error ε_ρ and the normalized chromaticity error $\varepsilon_{\bar{\rho}}$ were computed. All transformations were based on the sensor responses of the reconstruction set $\mathfrak{P}_\mathrm{R}$ as well as simulated sensor responses for the canonical illumination and color space derived from the spectral surface reflectivities of the same color patches. Therefore, the $\mathbf{XYZ}_\mathrm{CIE}$ color space and simulated daylight spectra for different *correlated color temperatures (CCT)*, computed according to [15], were used. Reference for comparison are *von Kries* adaption by scaling each color band independently, using a 3×3, and a 3×10 transformation matrix, respectively. All these transformations were found by linear regression between the sensor responses from the reconstruction set and the simulated canonical sensor responses. The 3×10 matrix includes quadratic terms within and between color channels similar to [3]. To be fair against these references, linearized measurements were used.

All error measures ε_ρ and $\varepsilon_{\bar{\rho}}$ between the transformed linearized measurements and the ideal canonical sensor responses have been compiled into Table 1. Each row represents a different canonical illuminant computed from the CIE daylights for CCT in the range 4000 K to 7000 K. The first column („None“) show the errors for uncorrected RGB, the second column (SPC-PE-Ma) contains results for the *SPC* algorithm with constrained principal eigenvector estimate for the sensor sensitivities as depicted in Figure 2(a). Further results were added with the sensor estimates of the quadratic programming algorithm [2] (SPC-QP-

Table 1: Experimental comparison of spectral color correction algorithm. The first column („None“) shows the errors for uncorrected RGB, the next two columns contain results for the spectral color correction algorithm with constrained principal eigenvector estimate (SPC-PE-Ma) and quadratic programming (SPC-QP-Ma). The last three columns contain results for von Kries adaption, 3×3 and 3×10 transformation matrices.

	None		**SPC-PE-Ma**		**SPC-QP-Ma**		**von Kries**		**Regr. 3×3**		**Regr. 3×10**	
CCT [K]	ε_ρ	$\varepsilon_{\bar{\rho}}$	ε_ρ	$\varepsilon_{\bar{\rho}}$	ε_ρ	$\varepsilon_{\bar{\rho}}$	ε_ρ	$\varepsilon_{\bar{\rho}}$	ε_ρ	$\varepsilon_{\bar{\rho}}$	ε_ρ	$\varepsilon_{\bar{\rho}}$
4000	19.63	0.116	3.02	0.039	4.83	0.047	9.11	0.086	3.05	0.038	3.08	0.038
4500	17.34	0.093	3.19	0.040	5.46	0.049	9.54	0.085	3.29	0.038	3.39	0.038
5000	15.96	0.081	3.37	0.040	6.06	0.050	9.94	0.084	3.51	0.038	3.67	0.038
5500	15.42	0.079	3.54	0.040	6.59	0.050	10.30	0.084	3.71	0.038	3.91	0.038
6000	15.51	0.083	3.70	0.040	7.07	0.051	10.62	0.084	3.88	0.039	4.12	0.038
6500	15.97	0.091	3.84	0.040	7.47	0.051	10.91	0.084	4.03	0.039	4.29	0.038
7000	16.60	0.100	3.97	0.040	7.83	0.051	11.16	0.084	4.16	0.039	4.44	0.039

Ma), displayed in Figure 2(b). In both cases, the Wiener inverse with Markov covariance matrix and $\rho = 0.99$ was applied. As predicted by the evaluation in Section 4, the errors are consistently higher than for the linear estimate.

Color correction performance of von Kries adaption exposed strong weaknesses in the present experiments with significantly higher errors. Regression with a 3×3 transformation performed comparably to the presented approach with similar errors $\varepsilon_{\bar{\rho}}$ in normalized chromaticity space, but higher absolute errors ε_ρ. The 3×10 transformation with quadratic terms performed a little worse than the 3×3 matrix and the spectral approach. This may have to do with instabilities or over-adaption due to the relatively sparse number of data points used for computation of the 30-element transformation matrix.

6 Discussion

The integrative spectral color correction framework presented in this work is able to estimate the illumination conditions of a scene from measurements of a color rendition chart and reproduces images under canonical conditions. The initial calibration of the system covers estimation of a linearization function and the sensor sensitivities from a reference color target under known illumination conditions.

The novelty of this approach lies in the generalization of the image formation model, allowing for linear pre-processing inside the camera system. Such transforms would lead to erroneous results with positivity constraint based algorithms or a monochromator based measurement. Compared with the works of [13, 7], where filter wheel cameras are used, this algorithm has to work with standard commercially available color cameras with a fixed number of filters and 8-bit resolution. This requires a linearization function so that the linear estimators can work.

The results presented in Section 5 also confirm the idea of not imposing a positivity constraint on such camera systems used in digital endoscopy systems. Compared with von Kries adaption, a clear advantage in terms of reproduction quality could be measured. Improvements were not as strong as compared to linear and polynomial regression based methods, but consistently noticable over the whole range of considered illuminants. Another advantage of the modular structure of the present approach is that each module can be optimized separately and even be exchanged, e.g. by non-linear spectrum estimators such as the ones presented in [5, 11, 14].

References

[1] K. Barnard and B. Funt. Camera calibration for color research. *Color Research and Application*, 27(3):153–164, 2002.

[2] G.D. Finlayson, S. Hordley, and P.M. Hubel. Recovering device sensitivities with quadratic programming. In *The Sixth Color Imaging Conference: Color Science, Systems and Applications*, pages 90–954, 1998.

[3] Jon Y. Hardeberg. *Acquisition and Reproduction of Color Images*. Dissertation.com, USA, 2001.

[4] F. König and W. Praefcke. A multispectral scanner. In L.W. MacDonald and M.R. Luo, editors, *Colour Imaging: Vision and Technology*, chapter 7, pages 129–143. John Wiley and Sons Ltd., 1999.

[5] R. Lenz, P. Meer, and M. Hauta-Kasari. Spectral based illumination estimation and color correction. *COLOR research and application*, 24(2):98–111, April 1999.

[6] Francisco Martínez-Verdú, Jaume Pujol, and Pascual Capilla. Calculation of the color matching functions of digital cameras from their complete spectral sensitivities. *J. Imaging Sci. Technol.*, 46(1):15–25, Jan./Feb. 2002.

[7] Y. Miyake, N. Tsumura, M. Takeya, and R. Inagawa. *Digital Color Imaging in Biomedicine*, chapter Applications of Color Image Processing Based on Spectral Information, pages 15–32. Digital Biocolor Society, 2001.

[8] C. Münzenmayer, D. Paulus, and T. Wittenberg. A spectral color correction framework for medical applications. *IEEE Trans. Biomed. Eng.*, 53(2):254–265, February 2006.

[9] D. Paulus, V. Hong, C. Idler, J. Hornegger, and L. Csink. Sensitivity curve approximation using linear algebra. In *CGIV 2004 – Second European Conference on Color in Graphics, Imaging and Vision*, volume 2, pages 207–212, Aachen, Germany, April 2004. The Society for Imaging Science and Technology.

[10] W.K. Pratt and C.E. Mancill. Spectral estimation techniques for the spectral calibration of a color image scanner. *Applied Optics*, 15(1):73–75, January 1976.

[11] A. Ribes and F. Schmitt. A fully automatic method for the reconstruction of spectral reflectance curves by using mixture density networks. *Pattern Recognition Letters*, 24:1691–1701, 2003.

[12] G. Sharma and H.J. Trussell. Set theoretic estimation in color scanner characterization. *Journal of Electronic Imaging*, 5(4):479–489, October 1996.

[13] T. Shiobara, S. Zhou, H. Haneishi, N Tsumura, and Y. Miyake. Improved color reproduction of electronic endoscopes. *J. Imaging Sci. Technol.*, 40(6):494–501, Nov./Dec. 1996.

[14] P. Urban and R.R. Grigat. Die Metamer-Randdeskriptor-Methode zur Farbkorrektur. In D. Droege and D. Paulus, editors, *10. Workshop Farbbildverarbeitung*, pages 1–9, Koblenz, 10 2004. Universität Koblenz-Landau, Der Andere Verlag.

[15] G. Wyszecki and W.S. Stiles. *Color Science: Concepts and Methods, Quantitative Data and Formulae*, chapter The CIE Colorimetric System. Wiley Series in pure and applied optics, 2nd edition edition, 1982.